Comparison of the dynamic response and environmental impact between traditional and innovative railway track systems

subgrade settlement [7]. Further, the ballasted track design has been used for over 150 years which implies that track engineers know what type of problems that can be expected and how to solve them.

In the decision process to determine whether slab track or ballasted track should be built, the dynamic response of the track is of great importance. Today, the dynamic response is often simulated by considering the train and track as one integrated system [8]. Depending on what type of response that shall be calculated, the adopted model varies. The most common approach is to model the vehicle as a multibody system (MBS) and the track using finite elements [9]. In recent years, the number of three-dimensional (3D) models have increased and several of the models have been calibrated and validated against measurement data [8,10–15].

The number of comparative studies between the dynamic performance of slab track versus ballasted track is limited. Bezin et al. [6] conducted simulations of the vertical dynamic vehicle–track interaction and compared ballasted track with a two-layer steel-concrete slab track and an embedded slab track. The simulations were conducted using the MBS software VI-Rail and all studied track designs were described using beams, springs and viscous dampers. From the simulations, the benefits of slab track in terms of local defects, e.g. the absence of hanging sleepers and less impact of localized weakened soil support, were verified. Blanco-Lorenzo et al. [16] compared ballasted track with the STEDEF track, RHEDA 2000 track and a floating slab track. In their study, different vehicle–track interaction models of varying complexity were considered, and conclusions of when a simpler model is applicable to use were presented. Chen et al. [17] used Green's functions to compare the dynamic performance of three different slab track designs frequently used in the Chinese railway infrastructure. From the comparison, significant differences in vertical displacement, acceleration and stress levels were found between the designs. Ntotsios et al. [18] conducted simulations in the wavenumber-frequency domain and compared levels of ground-borne vibration from slab track and ballasted track. From the study, it was concluded that there were only small differences in ground vibration levels between the two track designs. However, when using a softer rail pad stiffness in the slab track design, which is common practice to achieve a proper track stiffness at rail level, reduced vibration levels were observed above 63 Hz. Finally, Zhang et al. [19] compared sound radiation from slab track and ballasted track using an updated version of the so-called TWINS model. It was concluded that slab track is typically noisier, but the difference in sound radiation depends on what designs of slab track and ballasted track that are compared.

The number of comparative studies between ballasted track and slab track from an environmental point of view is also limited. Milford and Allwood [20] compared carbon dioxide (CO_2) emissions from ballasted track and potential future designs, such as embedded slab tracks. From the study, it was concluded that (independently of track design) the rail section is the component that contributes the most to CO_2 emission, and that it is important to maximize the time span of how long each track component can be in service. Du and Karoumi [21] conducted a life cycle assessment (LCA) of different railway track designs on bridges. The study included six impact categories: abiotic depletion potential, acidification potential, eutrophication potential, global warming potential, ozone layer depletion potential and photochemical oxidation potential. It was concluded that slab track has a better environmental performance on a bridge due to easier maintenance. Finally, Pons et al. [22] adopted the so-called ReCiPe (H) method to conduct LCA of ballasted track and slab track. The study concluded that the service life of the track designs affects which design is most environmentally friendly. As an example, when considering a service life of 50 years, the ballasted track would be the best option, whereas a slab track design may be preferred for service lives over 75 years.

In this paper, ballasted track is compared to a range of different slab track designs using an LCA and a methodology for simulation of three-dimensional (3D) vertical dynamic vehicle–track interaction. The considered slab track designs include (i) a design inspired by a system currently available on the market, (ii) an optimized slab track design based on the European standard 16432–2 [23], and (iii) an innovative slab track design using a ladder-type structure (3MB [24]). From the

dynamic model, the performance of the different designs are compared in terms of vertical wheel–rail contact forces, stresses in the concrete parts and pressures on the foundation. In addition, the LCA is used to compare the global warming potential from the different designs. From these comparisons, novel guidelines regarding the selection of track type are presented.

2. Selected railway track systems

In this paper, a ballasted track design and three different slab track designs are considered. The investigated slab track designs include (i) a design inspired by a system currently available on the market, (ii) an optimized slab track design based on the European standard 16432–2 [23] and (iii) the 3MB slab track [24]. In the decision process of which track systems that should be included in this study, it was prioritized to have a wide spread in track designs. In addition, systems that are well established on the market, as well as innovative systems with great potential, should be included.

In all of the designs, UIC60 rails are considered with bending stiffness $EI_r = 6.4$ MNm^2, shear stiffness $kGA_r = 250$ MN, mass $m_r = 60$ kg/m per unit length and rotatory inertia $m_r r_r^2 = 0.24$ kgm per unit length. Regarding the concrete parts, the density and Poisson's ratio are set to $\rho = 2500$ kg/m^3 and $\nu = 0.18$, respectively. Furthermore, the same soil stiffness (bed modulus), $k_f = 100$ MN/m^3, and soil damping (per unit area), $c_f = 82$ kNs/m^3, are used for all systems. Regarding the stiffness and viscous damping of each rail pad, different values are used for the ballasted track design and the slab track designs as this is common practice. The slab track systems have a rail pad stiffness and viscous damping of $k_{slab,rp} = 34$ kN/mm and $c_{slab,rp} = 5.8$ kNs/m [11], whereas the corresponding values for the ballasted track are $k_{bal,rp} = 120$ kN/mm and $c_{bal,rp} = 25$ kNs/m [25].

The ballasted track model sketched in Figure 1 contains rails, rail pads, sleepers and ballast/soil. The sleepers are assumed to be made of concrete with elastic modulus $E_s = 37$ GPa and the rail seat spacing is $L_{bal} = 0.60$ m.

The track inspired by a system currently available on the market, from now on referred to as the ST design, is sketched in Figure 2 and contains rails, rail pads, concrete panel, slab mats, roadbed and soil. Each concrete panel is modelled as a cuboid with width $b_{ST,p} = 2.4$ m, height

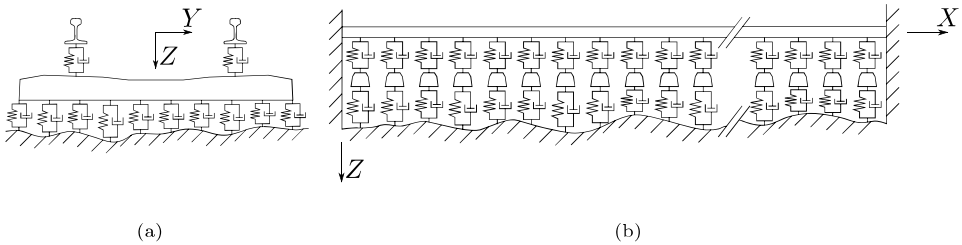

Figure 1. Sketch of ballasted track design. (a) Longitudinal view and (b) lateral view.

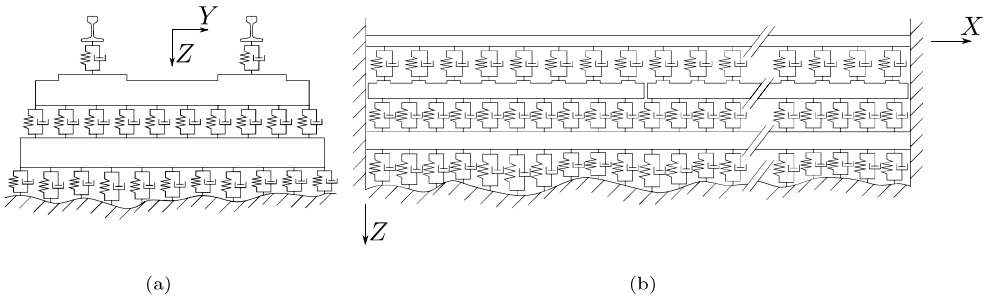

Figure 2. Sketch of ST and EN slab track designs. (a) Longitudinal view and (b) lateral view.

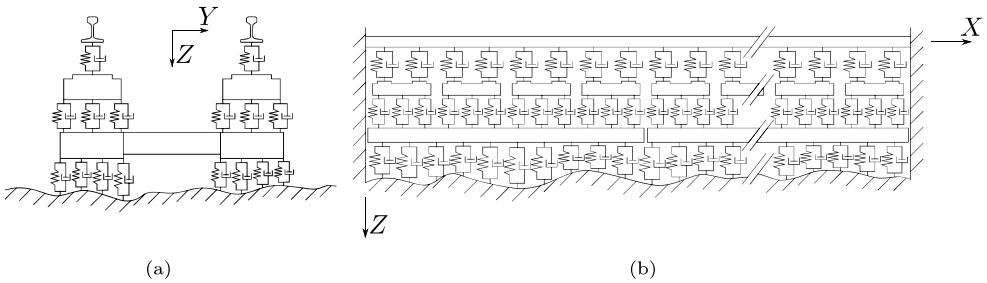

Figure 3. Sketch of 3MB slab track design. (a) Longitudinal view and (b) lateral view. For a top view of the discrete blocks on top of the slab base, see Figure 4.

$h_{\mathrm{ST,p}} = 0.16$ m and length $l_{\mathrm{ST,p}} = 5.2$ m (corresponding to eight rail seat distances). The panels are not coupled to each other but are supported by a common continuous reinforced concrete base layer (CBL) with width $b_{\mathrm{ST,r}} = 2.80$ m and height $h_{\mathrm{ST,r}} = 0.30$ m. In the ST design, a thin rubber mat (slab mat) is integrated on the bottom and in the openings of the panels. Here, the stiffness and viscous damping per unit area are set to $k_{\mathrm{ST}} = 1.0$ GN/m^3 and $c_{\mathrm{ST}} = 170$ kNs/m^3. Finally, the rail seat spacing is $L_{\mathrm{ST}} = 0.65$ m, while the elastic modulus of both panel and roadbed (CBL) is $E_{\mathrm{ST}} = 33$ GPa. It should be noted that different slab track designs may be used depending on in which country the slab track is installed and project-specific requirements. Alternative designs may alter the stiffness and damping of the rubber mat or the thickness of the CBL and may include a hydraulically bound layer (HBL) under the CBL. In this paper, prefabricated concrete panels on top of a CBL without any HBL is selected since this design seemed to be the most common one on open sections.

The slab track based on the European standard 16432–2 [23] was developed in Reference [26] with the objective to minimize the CO_2 emission from the concrete parts while still passing the standard. This slab track design is a (theoretically) optimized design from an environmental point of view and is not used in traffic today. There are several similarities between the ST design and the optimized design based on the European standard (from now on referred to as the EN design). As seen in Figure 2, both designs have prefabricated panels and a continuous concrete layer (CBL for the ST design and HBL for the EN design). In addition, the parameter values for the resilient layers are assumed to be the same for both designs. The concrete parts of the EN design have, however, different dimensions and physical properties compared to the ST design. The concrete panel has width $b_{\mathrm{EN,p}} = 2.60$ m, height $h_{\mathrm{EN,p}} = 0.19$ m and length $l_{\mathrm{EN,p}} = 4.80$ m, while the roadbed has width $b_{\mathrm{EN,r}} = 3.20$ m and height $h_{\mathrm{EN,r}} = 0.26$ m. In the EN design, the rail seat spacing is $L_{\mathrm{EN}} = 0.65$ m, while the elastic moduli of the panel and roadbed are $E_{\mathrm{EN,p}} = 31$ GPa and $E_{\mathrm{EN,r}} = 10$ GPa, respectively.

The final slab track design considered in this paper is the Moulded Modular Multi-Blocks (3MB) system developed by ACCIONA, CEMOSA, SYSTRA and INECO, see Figure 3. The slab track is a ladder-like structure with discrete top blocks resting on a slab base and is described in detail in References [24,27,28]. The slab base consists of two narrow slabs that are placed along with the rails. In addition, for each pair of narrow slabs, there are two beams in the lateral direction that connect the slabs to each other. In Figure 4, a top view of the top blocks mounted on the base is presented. Each discrete block is modelled as a cuboid with width $b_{\mathrm{3MB,bl}} = 0.55$ m, height $h_{\mathrm{3MB,bl}} = 0.2$ m and length $l_{\mathrm{3MB,bl}} = 1.00$ m. The height of each base slab is $h_{\mathrm{3MB,ba}} = 0.25$ m, while the narrow slabs have width $b_{\mathrm{3MB,ba}} = 0.60$ m and length $l_{\mathrm{3MB,ba}} = 4.80$ m. The beams that connect the slabs are not supported by the foundation and have width $b_{\mathrm{3MB,be}} = 0.30$ m and length $l_{\mathrm{3MB,be}} = 0.92$ m. The rail seat spacing is $L_{\mathrm{3MB}} = 0.60$ m and the elastic modulus of both block and base is $E_{\mathrm{3MB}} = 30$ GPa. Finally, the parameter values for the stiffness and viscous damping per unit area of the layer between the block and base are $k_{\mathrm{3MB}} = 0.25$ GN/m^3 and $c_{\mathrm{3MB}} = 43$ kNs/m^3.

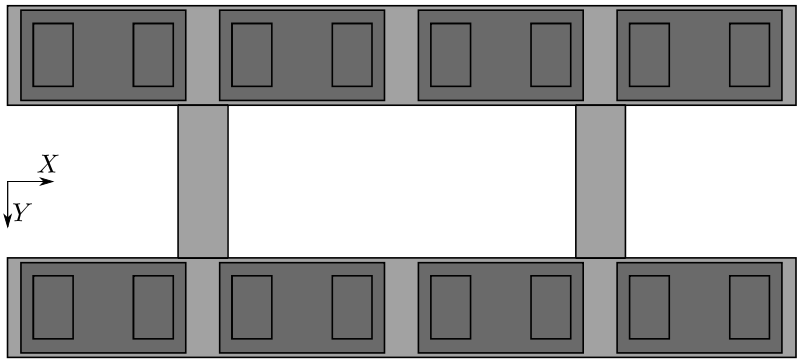

Figure 4. Top view of the discrete blocks on top of the slab base used in the 3MB design.

3. Methodology

In this paper, two independent methodologies are developed to compare the studied railway track forms in terms of (i) dynamic performance and (ii) environmental impact. The methodology for simulation of dynamic vehicle–track interaction is presented in Section 3.1, while the LCA is described in Section 3.2.

3.1. Dynamic vehicle–track interaction

The vertical dynamic vehicle–track interaction is simulated using a three-dimensional model that has been calibrated and validated against measurement data [11]. In the model, both of the rails and the sleepers are modelled as Rayleigh–Timoshenko beam elements, while the concrete panel, roadbed, block and base are modelled using shell elements. Since stresses will be evaluated in this paper, a quadratic shell element was chosen (denoted S8R in Abaqus). The finite element parts are connected using springs and viscous dampers, see Figures 1–3.

When the length of the track model is determined, there is a trade-off between accuracy and computational cost. Since the track models have different rail seat spacings, there is some deviation in the total track length. All studied track designs have, however, a length of 65–66 m. For such long track models, the influence of boundary effects on the track response at the centre of the track is small [29].

The track model is developed in Abaqus using Python scripts. Using Python scripts within Abaqus is a powerful tool to develop advanced track models. When the main script is executed, the stiffness, damping and mass matrices of the track ($\mathbf{K}^{\mathrm{t}}$, $\mathbf{C}^{\mathrm{t}}$ and $\mathbf{M}^{\mathrm{t}}$) are generated. These matrices are exported to Matlab where the vehicle model and the vehicle–track interaction code have been implemented. In order to reduce computational cost, the complex-valued modal solution of the equations of motion of the track is introduced as

$$\begin{bmatrix} \mathbf{K}^{\mathrm{t}^{-1}}\mathbf{C}^{\mathrm{t}} & \mathbf{K}^{\mathrm{t}^{-1}}\mathbf{M}^{\mathrm{t}} \\ -\mathbf{I} & \mathbf{0} \end{bmatrix} \begin{Bmatrix} \underline{\rho}^{(n)} \\ \mathrm{i}\underline{\omega}_n\underline{\rho}^{(n)} \end{Bmatrix} = -\frac{1}{\mathrm{i}\underline{\omega}_n} \begin{Bmatrix} \underline{\rho}^{(n)} \\ \mathrm{i}\underline{\omega}_n\underline{\rho}^{(n)} \end{Bmatrix}, \tag{1}$$

where $\underline{\omega}_n$ are the angular eigenfrequencies, $\underline{\rho}^{(n)}$ the eigenvectors, $\mathbf{I}$ denotes the unit matrix and underline indicates a complex-valued quantity. The computational cost is reduced by only including modes that have a corresponding eigenfrequency below a predefined threshold value. In this paper, modes with eigenfrequencies up to 1000 Hz have been included (except when a transient excitation due to a wheel flat was studied and eigenfrequencies up to 1500 Hz were included).

The vehicle is modelled as a three-dimensional multibody system and is sketched in Figure 5. In the model, the wheelsets and the bogie frame are modelled as rigid bodies and the primary suspension is modelled as a spring and viscous damper. The influence of the car body is added as

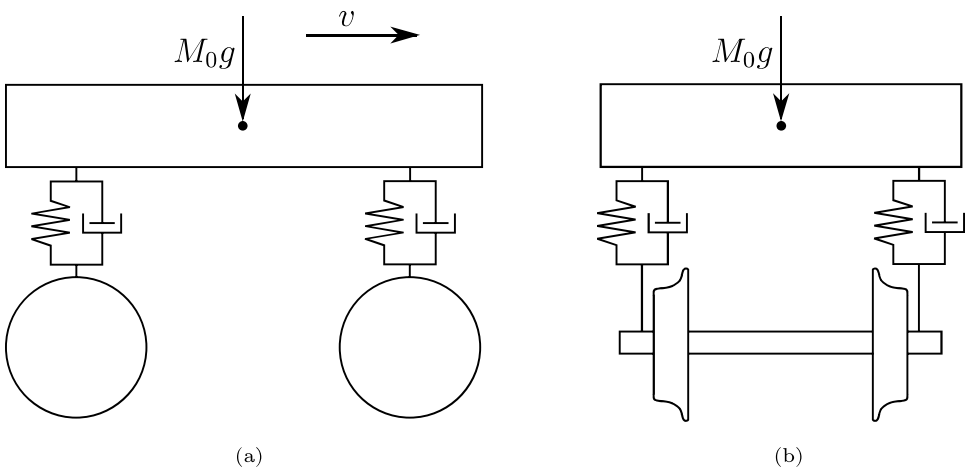

Figure 5. Sketch of vehicle model. (a) Side view and (b) end view. M_0 corresponds to the mass of half of the car body. Based on Figure 4 in Reference [26].

a static (constant) point force acting in the centroid of the bogie frame. From a previous study, cf. Reference [30], it has been verified that extending the vehicle model with a secondary suspension and a car body is not required when studying the dynamics of the track. The simplified bogie model gives accurate results as the secondary suspension acts as a dynamic filter isolating the car body from the bogie in the frequency range where the dynamics of the track is significant [31].

The parameter values for the vehicle model are presented in Table 1. These values were obtained from Reference [32] (except the mass of the car body which has been modified such that an axle load of 17 tonnes is obtained). In the table, the masses M_b, M_w and M_0 denote the masses of the bogie, wheelset and half of the car body, respectively, J_br and J_bp denote the roll and pitch inertias of the bogie, while J_wr denotes the roll inertia of the wheelset. The length Δ denotes the lateral distance from the centre of the track to the running circle of the wheel tread, whereas d_1 and d_2 denote the distances from the bogie centre of gravity to the primary suspension in the longitudinal and lateral directions. Finally, k and c denote stiffness and viscous damping of the primary suspension.

The vehicle model has eleven degrees of freedom (DOFs). Seven of these DOFs, $\mathbf{x}_\mathrm{b}^\mathrm{v}$, represent the ordinary physical DOFs of the model (vertical displacement, pitch and roll rotations of the bogie frame and vertical displacement and roll rotation of each wheelset). The remaining four DOFs, denoted $\mathbf{x}_\mathrm{a}^\mathrm{v}$, are (massless) vertical DOFs interfacing with the track and used in the constraint equations when the track and vehicle models are coupled [33]. The equations of motion for the vehicle can be written as

$$\begin{bmatrix} 0 & 0 \\ 0 & \mathbf{M}_\mathrm{bb}^\mathrm{v} \end{bmatrix} \begin{Bmatrix} \ddot{\boldsymbol{x}}_a^\mathrm{v}(t) \\ \ddot{\boldsymbol{x}}_b^\mathrm{v}(t) \end{Bmatrix} + \begin{bmatrix} 0 & 0 \\ 0 & \mathbf{C}_\mathrm{bb}^\mathrm{v} \end{bmatrix} \begin{Bmatrix} \dot{\boldsymbol{x}}_\mathrm{a}^\mathrm{v}(t) \\ \dot{\boldsymbol{x}}_\mathrm{b}^\mathrm{v}(t) \end{Bmatrix} + \begin{bmatrix} \mathbf{K}_\mathrm{aa}^\mathrm{v} & \mathbf{K}_\mathrm{ab}^\mathrm{v} \\ \mathbf{K}_\mathrm{ba}^\mathrm{v} & \mathbf{K}_\mathrm{bb}^\mathrm{v} \end{bmatrix} \begin{Bmatrix} \boldsymbol{x}_\mathrm{a}^\mathrm{v}(t) \\ \boldsymbol{x}_\mathrm{b}^\mathrm{v}(t) \end{Bmatrix} + \begin{Bmatrix} \mathbf{F}_\mathrm{a}(t) \\ 0 \end{Bmatrix} = \begin{Bmatrix} 0 \\ \mathbf{F}_\mathrm{b}^\mathrm{ext} \end{Bmatrix}, \tag{2}$$

Table 1. Parameter values used in the vehicle model collected from Reference [32] (except M_0).

$M_\mathrm{b} = 2.6$ tonnes	$M_\mathrm{w} = 1.8$ tonnes	$M_0 = 28$ tonnes
$J_\mathrm{br} = 1700$ kgm^2	$J_\mathrm{bp} = 1500$ kgm^2	$J_\mathrm{wr} = 1100$ kgm^2
$\Delta = 0.75$ m	$d_1 = 1.28$ m	$d_2 = 1.00$ m
$k = 1200$ kN/m	$c = 4$ kNs/m	

where $\mathbf{K}_{bb}^{v}$, $\mathbf{C}_{bb}^{v}$ and $\mathbf{M}_{bb}^{v}$ denote the stiffness, damping and mass matrices of the vehicle model, $\mathbf{F}_a$ contains the time-varying vertical wheel–rail contact forces and $\mathbf{F}_b^{ext}$ contains the external loads (in this study only gravity loads). The expression of each sub-matrix in Equation (2) can be found in Appendix A in Reference [29]. In this study, non-linear Hertzian springs are used to model each contact between wheel and rail. The contact stiffness is given by

$$k_{Hi} = C_H \langle x_{bi} - x_{ai} \rangle^{1/2}, \quad i = 1, 2, 3, 4, \tag{3}$$

where C_H is the Hertzian constant and the Macaulay brackets are defined as $\langle \bullet \rangle = \frac{1}{2}(\bullet + |\bullet|)$.

By utilizing that $\mathbf{x}_a^v$ is interfacing with the track, the vehicle model is coupled to the modal representation of the track [34,35]. A mixed extended state-space vector $\underline{\mathbf{z}}$ is defined as

$$\underline{\mathbf{z}} = \{\underline{\mathbf{q}}^{tT} \;\; \boldsymbol{x}_a^{vT} \;\; \boldsymbol{x}_b^{vT} \;\; \dot{\boldsymbol{x}}_a^{vT} \;\; \dot{\boldsymbol{x}}_b^{vT} \;\; \hat{\boldsymbol{F}}_a^{T}\}^{T}, \tag{4}$$

where $\underline{\mathbf{q}}^{tT}$ is the modal displacement of the track and $\hat{\boldsymbol{F}}_a = \int \boldsymbol{F}_a(t)\mathrm{d}t$. This state-space vector is used to derive a coupled, time-variant system which is given by

$$\underline{\boldsymbol{A}}(\underline{\boldsymbol{z}}, t)\,\dot{\underline{\boldsymbol{z}}} + \underline{\boldsymbol{B}}(\underline{\boldsymbol{z}}, t)\underline{\boldsymbol{z}} = \underline{\boldsymbol{F}}(\underline{\boldsymbol{z}}, t), \tag{5}$$

where the vector $\underline{\boldsymbol{F}}$ and the matrices $\underline{\boldsymbol{A}}$ and $\underline{\boldsymbol{B}}$ are defined in Equation (15) in Reference [35]. From Equation (5), an initial value problem is established, which can be solved numerically in the time domain. In this paper, an adaptive time step is used in the numerical solver, but the response is extracted using a (constant) time step of $\Delta T = 10^{-4}$ s (except in the simulations that contain a wheel flat where the time step is reduced due to the high-frequent excitation).

By differentiating the calculated state-space vector, the time-history of the wheel–rail contact force between each wheel and rail is determined. These forces are used as input to a post-processing simulation in Abaqus where additional track responses are calculated. The influence of the wheel–rail contact forces is added in the Abaqus model by applying time-variant forces and moments to the rail DOFs that are adjacent to each wheel–rail contact. For consistency, the magnitude of each force and moment that shall be applied in each time instant is calculated using the shape functions from Rayleigh–Timoshenko beam theory.

In Figure 6, the simulation methodology is summarized. In addition, the software used in each step is indicated. The simulation methodology is further described in References [29,34,35].

When including track irregularities in the track model, wavelengths in the interval $1 - 25$ m have been generated using the Power Spectral Density (PSD) function according to Claus and Schiehlen [36]. The irregularities on the two rails are assumed to be uncorrelated and induce a non-symmetric excitation. Track quality can, according to the European standard 13848–6 [37], be divided into different track classes depending on the standard deviation of the irregularity (ranging from A to E). In order to have a realistic magnitude of the irregularities generated from the PSD, the magnitude was scaled such that the standard deviation of the irregularities in longitudinal level corresponded to the limit value specified for track class C. Using track class C can be seen as a worst-case scenario for high-speed applications [26]. At vehicle speed 250 km/h, which has been

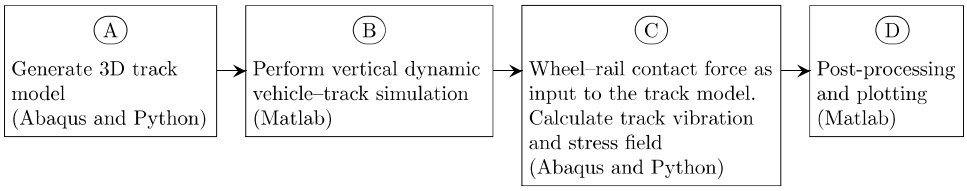

Figure 6. Flowchart of the different steps in the simulation methodology.

studied in this paper, the applied rail irregularities generate a dynamic excitation in the frequency range $3 - 69$ Hz. For more information about the generation of track irregularities as input to the model, see Reference [26].

When the selected PSD is applied to generate the irregularities in track geometry, a relatively low-frequent dynamic excitation is induced, where frequencies in the interval $30 - 40$ Hz dominate the contribution to the wheel–rail contact forces. As an alternative to the irregularities generated by the PSD, simulations where the track is excited by a wheel flat have also been conducted. Compared to the PSD, a wheel flat generates a more transient excitation where higher frequencies will dominate the response. Therefore, additional modes (with corresponding eigenfrequencies up to 1.5 kHz) were used in the simulations. In addition, the output was sampled more frequently with a time step of $\Delta T = 10^{-5}$ s in the numerical solver. When the wheel flat was modelled, the finite curvature of the wheel was taken into account as proposed by Wu and Thompson [38]. The relation between the initial length, l_{wf}, and depth, d_{wf}, of the wheel flat was found from the intersecting chords theorem. However, due to the rounding of edges that is created from plastic deformations and wear, the length of the wheel flat used in the simulations was increased by 50% compared to the initial length. Finally, the wheel flat was assumed to be located on either one or both wheels of the leading wheelset, which implies that both symmetric and non-symmetric excitations have been studied.

As a complement to the dynamic vehicle–track interaction simulations, also static simulations have been conducted to calculate the track stiffness at rail level for the different track designs. The static stiffness is calculated by applying vertical unit loads on the two rail nodes in the FE-model that have the same longitudinal track coordinate. From the obtained displacement field, the displacement at the location of the loads is determined, and the static stiffness is obtained by taking the ratio between the load and the displacement. By repeating the calculations for each rail node, the variation in static stiffness along the track is found.

3.2. Environmental impact

In this paper, the developed LCA is focused on the global warming potential. Hence, the associated CO_2 emission from the life cycle is calculated for each railway track design. When the CO_2 emissions are to be calculated, the contribution from the track is usually divided into three main stages: construction, maintenance and end-of-life [20]. The LCA is limited to the emissions from the track designs as the influence of emissions due to for example stations and rolling stock is considered to be outside of the scope of the paper.

Within the construction phase, the main CO_2 emissions are produced from the production of the parts, construction machinery and material transportation. The emissions due to transportation of components during construction vary depending on the required transportation distance. However, the emissions due to transportation of components have been shown to be low compared to the overall emissions. As an example, when assuming that all components need to be transported 200 km, the associated emissions are less than 3% of the overall emissions [20]. Similar values were provided in the study by Pons et al [22], which concluded that the contribution of CO_2 emissions due to transport of materials, construction machinery and operations required to build the infrastructure is around 4%. Hence, the environmental impacts of construction machinery and material transportation are neglected in this study. Finally, the impact of subsoil improvements, which would have an environmental impact and would vary from site to site, is outside the scope of this paper.

When considering the production of the parts required in the track designs, the focus is on the rails, concrete parts, reinforcement and ballast since these are the components that produce the most CO_2 emissions [22]. The emissions from the production of the rail section are obtained by multiplying the mass of the rails with the scaling factor $\alpha_s = 2.63$ kg CO_2 per kg steel [39]. When considering emissions related to reinforced concrete, the influence of cement and reinforcement, which are the most prominent parts, are both taken into account. The influence of other material/processes during the production

Table 2. Amount of cement per cubic metre of concrete.

	Sleeper	ST	EN panel	EN roadbed	3MB
Cement content [kg/m^3]	430	330	290	75	390

of reinforced concrete, e.g. the energy during production, is small compared to the emissions due to cement and steel and is therefore neglected in this study. The emissions due to the reinforcement bars are calculated in a similar way as for the rail steel, but with another scaling factor ($\alpha_r = 0.55$ kg CO_2 per kg steel) since another type of steel is used compared to the rails [40]. The amount of cement per cubic metre of concrete is shown in Table 2. In the table, different values are specified for the different designs since different types of concrete are used. For the ST design and the 3MB design, the same type of concrete is used in both layers. In contrast, the bottom layer in the EN design is an HBL which has a very low cement content. From the geometric dimensions of the track designs and the concentrations of cement per unit volume, the total amount of cement is calculated. Finally, the CO_2 emissions due to the concrete is calculated by multiplying the amount of cement with the scaling factor $\alpha_c = 0.68$ kg CO_2 per kg cement [41]. In this paper, the scaling factors α_s, α_r and α_c have been obtained from representative Environmental Product Declaration (EPD) documents [39–41].

In the maintenance phase, the main emissions are due to track renewal. Hence, the life of each component affects the results significantly. In this paper, the life of the rails is assumed to be 40 years, independently of track design. The sleepers are assumed to also have a life of 40 years, whereas the life of the slabs is set to 80 years. In practice, the design life of the concrete slab may vary between different projects. It has been verified that the adopted lifetimes are in the correct order of magnitude. Other maintenance activities include rail grinding and tamping. Rail grinding is assumed to be required for all track designs, whereas tamping is only performed on the ballasted track. Based on mean values of numbers reported in Reference [20], it is assumed that rail grinding emits 1.0 kg CO_2 per metre track and occurs at intervals of 3.3 years. Similarly, tamping is assumed to emit 0.153 kg CO_2 per metre track and occurs at intervals of 1.3 years.

In the end-of-life phase, there will be some emissions due to track dismantling, transport and disposal. The emissions from this phase are, however, small compared to the overall emissions ($< 2\%$ cf. [22]) and are therefore neglected in this paper.

4. Results

The selected track designs are compared in terms of both track performance and environmental impact. The results from the investigation of track performance, presented in Section 4.1, focus on critical responses such as vertical wheel–rail contact force on tangent track, stresses in the concrete parts and pressures on the foundation. To enable a comparison of the performance, the same representative load cases have been applied to all track designs. This includes the assumption of the same uniform bed modulus of the supporting foundation for all track models, and the selection of two characteristic types of wheel–rail contact loading due to either a PSD of vertical track irregularity representing a dynamic excitation in a given frequency interval or a discrete wheel irregularity inducing a transient excitation. Further, the same vehicle speed (250 km/h) and axle load (17 tonnes) have been applied in all simulations. The results related to the environmental impact, see Section 4.2, focus on the global warming potential from an LCA perspective.

4.1. Track performance

Similarities and differences between the four track designs have been analysed using both static and dynamic analyses. In Figure 7(a), the vertical static track stiffness at rail level is presented as a function of longitudinal track coordinate. All track designs have a periodic pattern due to the

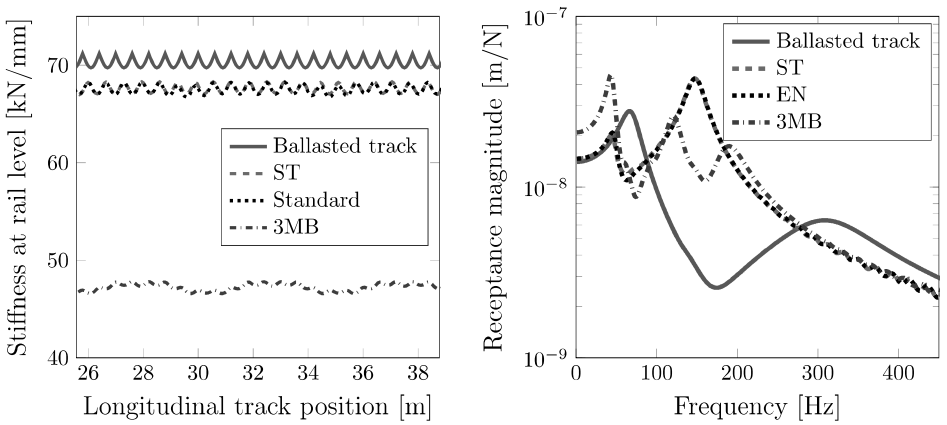

Figure 7. (a) Static stiffness at the rail level and (b) point receptance on the rail on top of a rail seat.

discrete positions of the rail seats. Furthermore, it is noted that the stiffness of the 3MB system is significantly lower than the stiffness of the other systems. Even though the same rail pad stiffness and foundation bed modulus have been used in all slab track designs, the 3MB system is more flexible since the base area in contact with the soil is smaller compared to the other slab track designs. In addition, a lower stiffness between the block and base is used compared to the stiffness between panel and roadbed, which reduces the stiffness at rail level even further. The low static stiffness for the 3MB system may be problematic if the track is combined with another track since the generated stiffness gradient at the transition may increase dynamic loads and the risk of differential settlement. Finally, a variation in stiffness along the longitudinal track position is noted for all slab track designs due to the discrete concrete parts (in particular for the 3MB system).

The difference in static track stiffness at rail level is also seen in Figure 7(b), where the vertical point-receptance on the rail is shown for the different designs. As expected in the studied frequency interval, two peaks (resonances) can be seen for the ballasted track. At the first resonance, the sleepers and rails move principally in phase, while they move out of phase at the second resonance. In agreement with a previous study, cf. Reference [35], two resonances can also be seen for the ST design and the EN design. In contrast, three resonances can be observed for the 3MB system. The first and third of these resonances correspond to the same types of vibration modes that can be identified for the other designs. At the second resonance, the rails and blocks move principally in phase, and out of phase with the base slabs. There are several reasons why this resonance can be seen for the 3MB system but not for the other slab track designs. The main reasons are the significantly lower stiffness and damping between block and base in the 3MB design and the fact that the block has a lower mass than the panels. If the stiffness between panel and roadbed would be reduced significantly, then three resonances would appear in the studied frequency interval also for the ST and EN designs. Above the studied frequency interval, all of the designs have similar receptance magnitudes (except around the pinned-pinned mode for which the resonance frequency is slightly shifted between the designs due to different rail seat spacings).

The simulations of the static response show that there are significant differences between the designs that need to be analysed further. This has been done using simulations of vertical dynamic vehicle–track interaction. Since the dynamic performance between the different track designs may vary depending on the randomly selected track irregularities, several simulations have been conducted with different realizations of the irregularities. In Figure 8(a), normal distributions of the vertical wheel–rail contact

force have been determined based on calculated time histories from 30 different realizations of track irregularities in the simulations. The irregularities were generated using the PSD described in Section 3.1. From the figure, it is seen that there is a spread in the variance of wheel–rail contact force between the different designs. It is concluded that an advantageous response with a lower variance is obtained for the ballasted track. Based on a Fourier transform of the calculated wheel–rail contact forces, it was (as expected) found that the frequency interval $3-69$ Hz dominated the time-history of the wheel–rail contact force. By increasing the wavelength interval used in the PSD, additional simulations have been conducted to study the influence of excitations of higher frequencies. From these simulations (not shown here), it was found that frequencies above 69 Hz do not have a significant influence on the fitted normal distributions of the vertical wheel–rail contact force for the different designs.

For a stationary harmonic excitation, the amplitude of the vertical wheel–rail contact force is proportional to the inverse of the magnitude of the system receptance evaluated at the wheel–rail contact [42,43]. For all of the studied track designs, the system receptance has been calculated by summing the receptances from the track and vehicle models, see Reference [35]. In Figure 8(b), these system receptances are shown for the frequency interval where the rail irregularities induce a dynamic excitation. From the figure, it is seen that all track designs have a local minimum in the system receptance between $30-40$ Hz. It can be observed that the level of the local minimum is slightly lower for the ST and EN designs, which increases the dynamic part of the vertical wheel–rail contact forces. In addition, it is noted that the magnitude of the system receptance is significantly larger for the ballasted track and the 3MB system above 50 Hz. This implies that the magnitudes of the dynamic part of the time-variant vertical wheel–rail contact forces are smaller for the ballasted track and the 3MB system designs above 50 Hz leading to an overall lower standard deviation.

In Figure 9, the distribution of maximum pressure on the foundation is shown for all different designs. As described in detail in Reference [29], the distributions were calculated by extracting the maximum value from the time-history of the pressure for each spatial position that is in contact with the foundation. To limit the computational cost, the distributions of maximum pressure were calculated for one load case when using one realization of the irregularity profiles that give a similar normal distribution as when all 30 realizations were taken into account. As expected, non-symmetric pressure distributions can be seen in Figure 9 since different irregularities have been applied to the two rails. When comparing the different track designs, it is seen that the ballasted track generates the highest pressure levels on its foundation, which is disadvantageous from

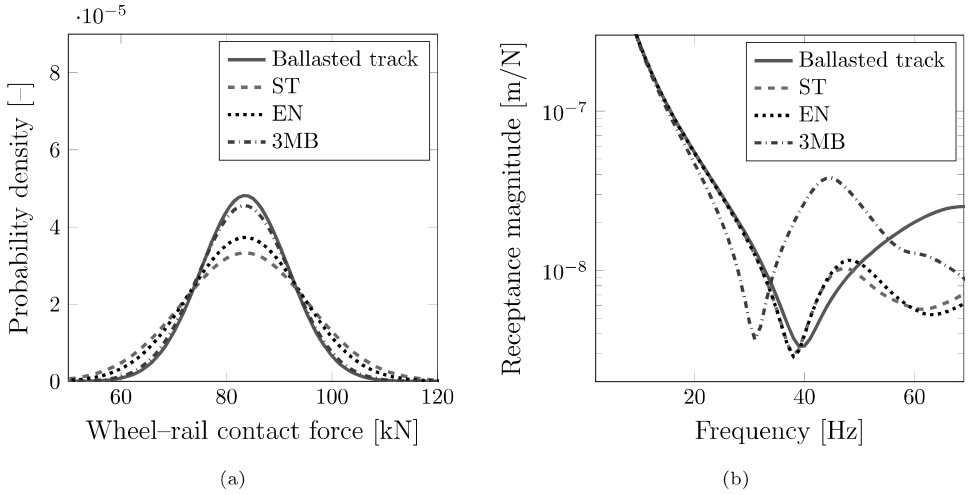

Figure 8. (a) Fitted normal distribution of the vertical wheel–rail contact force when taking all wheels and realizations into account. (b) Magnitude of system receptance.

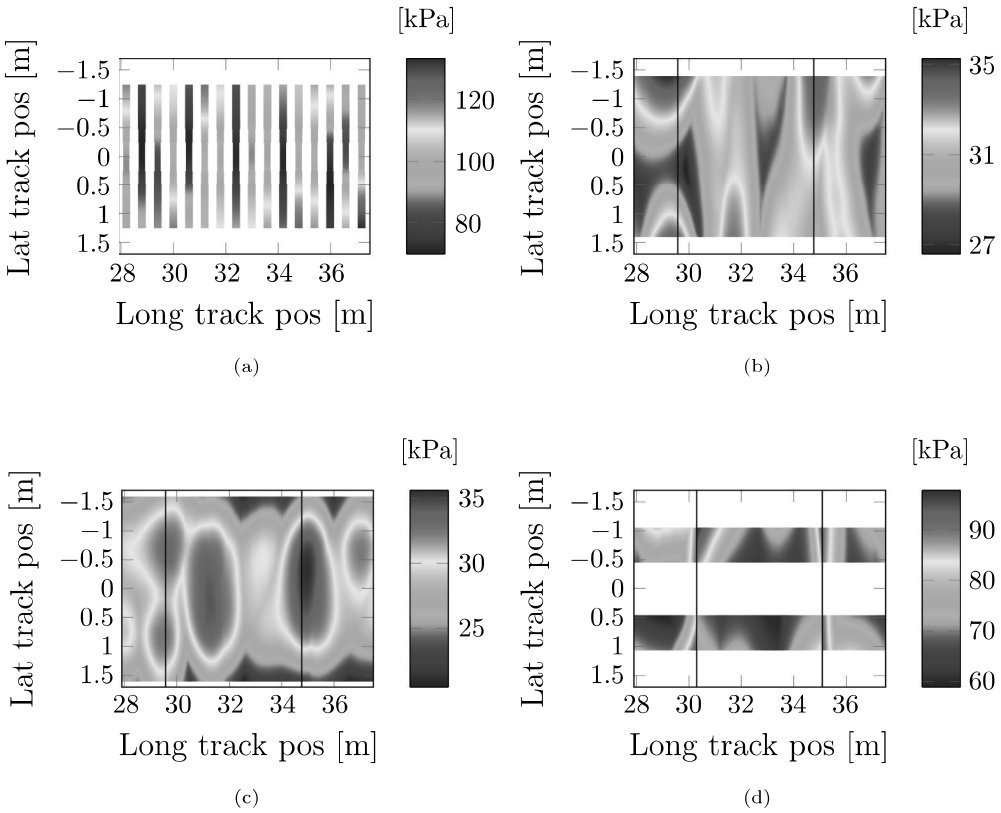

Figure 9. Distribution of maximum pressure on the supporting foundation for (a) ballasted track design (b) ST design (c) EN design and (d) 3MB design. Note the difference in scale for the colour bar between the different designs. In (b) and (c), the vertical black lines indicate the locations where two panels meet, and in (d), these lines correspond to the locations where two base slabs meet. The same realization of track irregularity has been applied for all track designs.

a durability point of view since increased pressures increase the risk of ballast degradation and overall settlement of the foundation. The main reason for the pressure increase is the much smaller contact area to the foundation for a ballasted track compared to a slab track design. However, it should be noted that the ballast will distribute the load to the substructure leading to a reduced value at the interface between ballast and substructure.

When comparing the pressure distributions from the slab track systems in Figure 9, it is noted that the 3MB system induces significantly larger pressures compared to the other slab track designs. The main reasons for this are (i) smaller base area in contact with the foundation and (ii) discrete base elements in the 3MB design versus a continuous layer in the other slab track designs. The benefit of having a continuous bottom layer is clear in Figures 9(b-c) since no significant pressure increase is noted where the panels meet. The disadvantageous periodically increased pressure levels for the 3MB system increase the risk of differential track settlement. Finally, it is noted that the maximum pressure tends to occur on the edge of the roadbed for the ST design. In contrast, the maximum pressure tends to occur more centrally for the EN design, since it has a slightly wider roadbed compared to the ST design.

In Figures 10 and 11, the maximum bending tensile stress is shown for the different systems. The stresses for the sleepers in the ballasted track is shown in Figure 10 and are calculated by extracting the bending moments from the dynamic model that give tensile stresses for each lateral position and applying Navier's formula. As expected due to the assumption of uniform support conditions along each sleeper, it is seen that the stresses have their maximum at sleeper centre. At these locations, the

tensile stress occurs at the top surface of the sleepers. In addition, local stress concentrations can also be seen below the rails. In contrast to the stresses at sleeper centre, these local stress concentrations cause tensile stresses at the bottom surfaces of the sleepers. By using a varying bed modulus with reduced stiffness at the sleeper centre due to proper tamping, the stress level at the centre can be reduced [44].

When comparing the slab track designs, see Figure 11, there are both similarities and differences. For all the designs, stress concentrations can be seen in the upper layer below the rail seats. An advantage of the 3MB system is that the magnitude of these stress concentrations is significantly lower compared to the other slab track designs due to the smaller size of the discrete blocks.

When studying the stress distributions of the lower concrete layer, it is seen that the stress magnitudes are the lowest for the EN design in which a relatively soft concrete base (HBL) is used. For the 3MB design, the stresses in the base are significantly higher than the corresponding stresses in the roadbed in the other designs. The main reason is due to the geometry of the base and the fact the concrete panels can distribute the load by bending to a larger degree than the individual blocks used in the 3MB design. As expected, stress concentrations can be seen at the corners of the base where the beams are mounted in the 3MB design. The magnitude of these stress concentrations is, however, not very large. In addition, a small rounding of 5.5 mm (which is not modelled in this paper) is typically included which reduces the stress concentration even further.

From Figure 10 and Figure 11(a) range of different maximum stresses are found. To investigate the risk of crack initiation, the maximum value can be compared with the maximum flexural tensile strength. According to Eurocode 2 [45], the mean flexural tensile strength can be determined as

$$f_{\mathrm{ctm,fl}} = \max((1.6 - h)f_{\mathrm{ctm}},\, f_{\mathrm{ctm}}), \tag{6}$$

where f_{ctm} is the mean axial tensile strength of the concrete and h is the thickness of the concrete part given in metres. In Table 3, the ratio between the maximum bending stress, $\sigma_{\max}$, and the mean flexural tensile strength is shown for all track designs. From the table, it is noted that the maximum stresses in all concrete parts are below the mean flexural tensile strength meaning that no cracks will form. In particular, relatively small ratios are found for the bottom layer of the ST design and the concrete blocks used in the 3MB design. For these parts, there may be a possibility to reduce the thicknesses and save environmental and monetary costs.

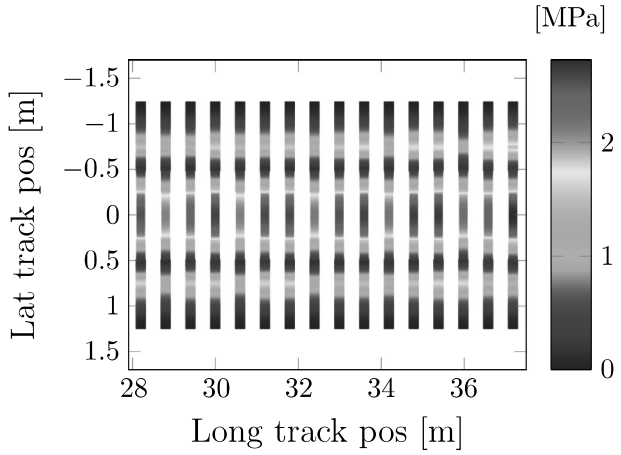

Figure 10. Distribution of maximum tensile stress for the sleepers in the ballasted track.

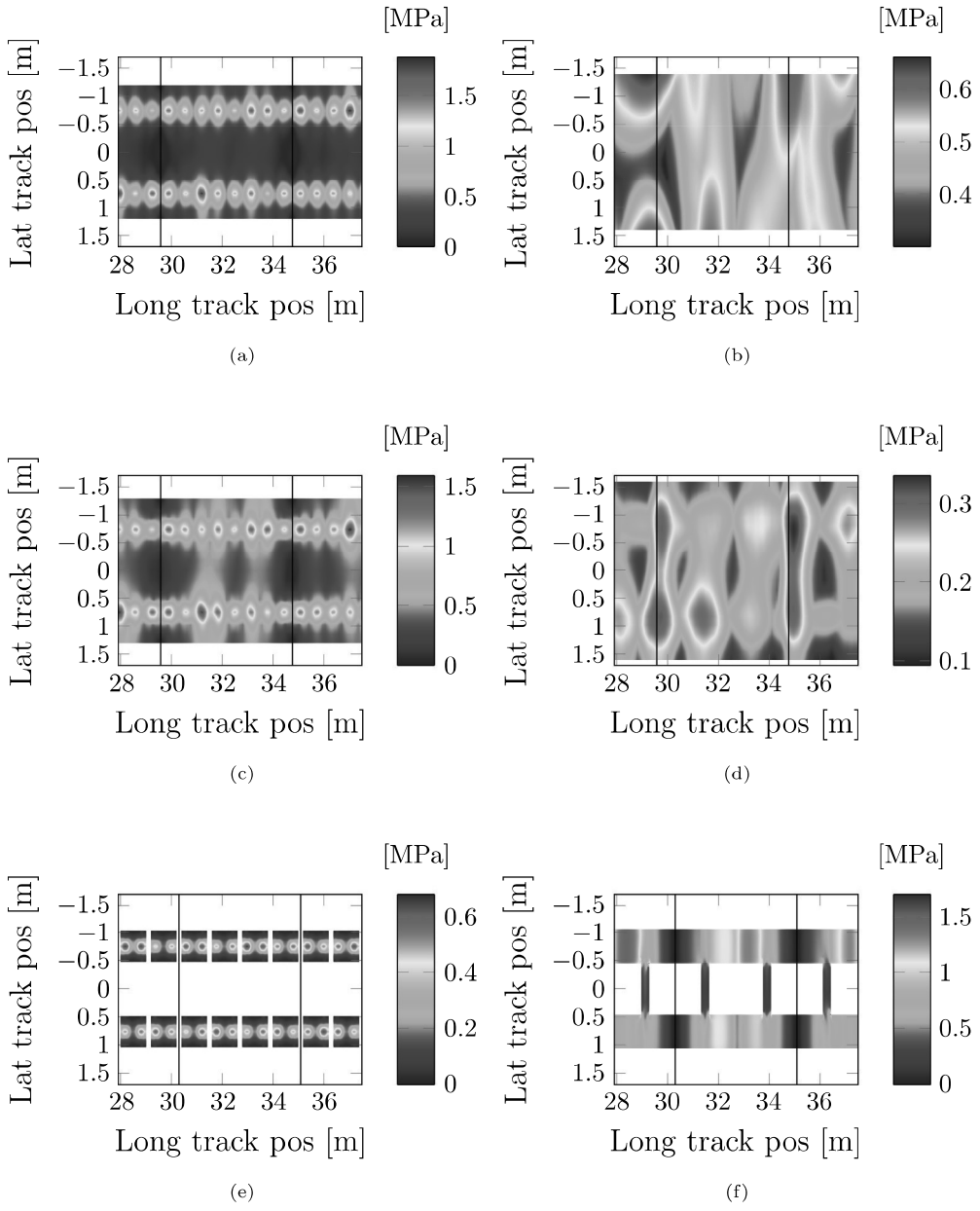

Figure 11. Distribution of maximum principal stress for (a) ST panel (b) ST roadbed (c) EN panel, (d) EN roadbed, (e) 3MB block and (f) 3MB base. Note the difference in scale for the colour bar between the different designs. In (a)–(d), the vertical black lines indicate the locations where two panels meet, while in (e)–(f), these lines correspond to the locations where two base slabs meet.

Table 3. Ratio between maximum bending tensile stress and mean flexural tensile strength.

	Ballasted	ST panel	ST CBL	EN panel	3MB block	3MB base
Ratio $\sigma_{max}/f_{ctm,fl}$ [–]	47%	45%	18%	44%	14%	36%

In Figure 12, the maximum wheel–rail contact force for the different designs is shown as a function of the depth of the wheel flat. From the figure, it is noted that the symmetric and non-symmetric excitations lead to similar results. It is also concluded that all slab track designs give

similar maximum wheel–rail contact forces, whereas the ballasted track design gives slightly lower values. The main reason for the reduced values for the ballasted track design is the different rail pad stiffness. The studied range of wheel flat depths generates time-histories of the wheel–rail contact force that include both continuous wheel–rail contact and cases with momentary loss-of-contact. Depending on the track design, loss-of-contact starts to occur for depths of $0.18 - 0.19$ mm. Above 0.10 mm depth, it is seen that the increase in maximum wheel–rail contact force with increasing depth is fairly linear until loss-of-contact occurs where the rate of increase starts to decrease. The magnitudes of the maximum wheel–rail contact forces are slightly larger than the corresponding values reported in Reference [46], meaning that the models adopted in this paper give conservative results. The main reason for this is the simplified wheelset model which leads to an increased dynamic stiffness at high frequencies [25]. In addition to the wheel–rail contact forces, the maximum bending moment in the rails has been evaluated. From this analysis, it was concluded that similar maximum values were obtained for all designs.

The corresponding maximum stress levels in the concrete parts and the maximum pressures on the foundation have also been calculated. In Table 4, the maximum stresses are listed for the different designs considering the non-symmetric excitation and two different wheel flat depths. The selected depths correspond to one case with continuous wheel–rail contact and one case with momentary loss-of-contact. By comparing the stress levels for the two depths, it can be seen that similar magnitudes are obtained for the different slab track designs, whereas a significantly increased maximum stress is obtained for the larger depth for the ballasted track design. The reason for this difference between the designs is the difference in rail pad stiffness. For the softer pad, which is used in the slab track designs, the dynamic decoupling between the rail and the concrete parts occurs at a lower frequency. This means that more of the high-frequency load excitation caused by the wheel flat is filtered out by the softer rail pad. Although the stresses are significantly higher for the ballasted track, it should be noted that the stresses are still below the maximum flexural tensile strength. Finally, Table 5 shows the

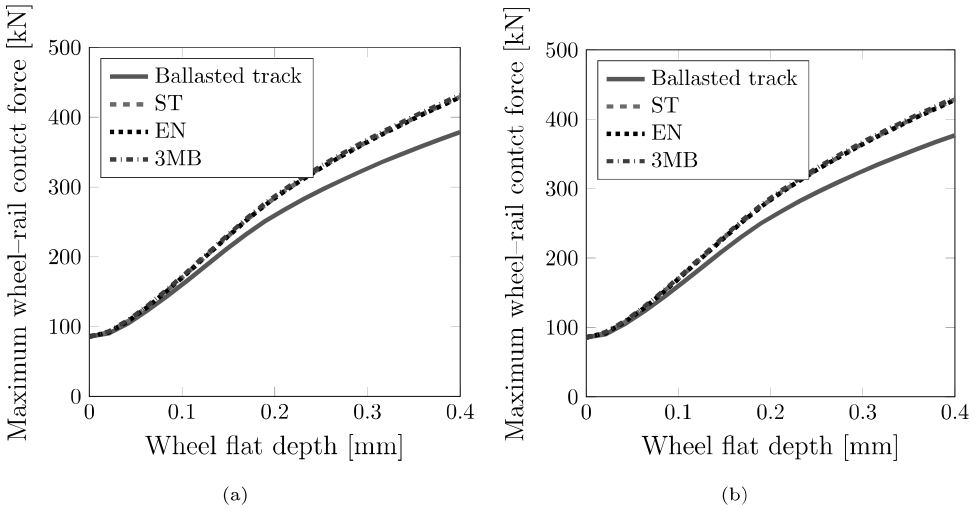

Figure 12. Maximum wheel–rail contact force considering (a) wheel flats on both of the wheels on the leading wheelset (symmetric excitation) and (b) wheel flat only on the leading right wheel (non-symmetric excitation).

Table 4. Maximum bending tensile stress for two different wheel flat depths.

	Ballasted	ST panel	ST CBL	EN panel	3MB block	3MB base
Max stress [MPa] $d_{wf} = 0.1$ mm	2.5	1.3	0.4	1.1	0.6	1.0
Max stress [MPa] $d_{wf} = 0.3$ mm	3.3	1.4	0.4	1.2	0.7	1.0

Table 5. Maximum pressure on the foundation for two different wheel flat depths.

	Ballasted	ST	EN	3MB
Max pressure [kPa] $d_{wf} = 0.1$ mm	99	26	26	82
Max pressure [kPa] $d_{wf} = 0.3$ mm	106	26	26	82

maximum pressure on the foundation for the different designs and wheel flat depths. Similar to the stress magnitudes, it is noted that similar pressure levels are obtained for both depths when considering the slab track designs, whereas an increase is noted for the ballasted track design.

4.2. Environmental impact

The methodology described in Section 3.2 is used to compare the environmental impact from the studied track designs. In Table 6, the total CO_2 emissions per metre built track and year is shown. By comparing the environmental impact from the different designs, a significant difference is noted. It is noted that the ballasted track and the 3MB track generate similar CO_2 emissions, while the ST design has the largest impact since it uses two layers of reinforced concrete. The main reason why the difference in emissions between the ballasted track design and the slab track designs is not larger is due to the assumed significantly shorter service life of the sleepers compared to the slabs. It should be noted that the emissions from the ST design are calculated based on a track on open sections. If the track would be installed in a tunnel, the emissions from the concrete and reinforcement parts would be reduced since the CBL is not required in tunnels.

In Figure 13, it is analysed which parts of the LCA that produces the most CO_2 emissions. As expected, it can be seen that the production of the rails produces the most emissions followed by the production of the concrete. From the figure, it is clear that the maintenance activities (not including track renewal) have only a small impact. Since the production of the rail steel is the dominating part for all designs, a significant CO_2 saving would be obtained if the service life of the rails could be extended or if another rail design could be used with less environmental impact. Although the rail is the part that emits the most CO_2 emissions, there is still significant contributions from the concrete parts. In Table 6, the CO_2 emissions from the concrete and reinforcement are shown. Here, the difference in emissions between the designs is clearly seen, where the emissions from the ST design are the highest since the design uses two layers of reinforced concrete.

Since the production of steel and concrete are the processes that emit the most CO_2 emissions, the environmental impact of building a railway track is significant. However, depending on what type of track design is built, the ratio between the impact from construction and renewal varies. In Figure 14, the construction of the track is compared with renewal and other maintenance activities (i.e. rail grinding and tamping). In the figure, a difference is noted between the ballasted track design and the slab track designs, where the ballasted track tends to have a larger part associated with environmental impact due to renewal. The main reason for this is the longer service life of the concrete slabs compared to the concrete sleepers.

Table 6. Comparison of (i) total CO_2 in kg per metre and year and (ii) CO_2 emission from concrete and reinforcement in kg per metre and year for the different track designs.

	Ballasted	ST	EN	3MB
CO_2 total [kg/(m year)]	10.5	13.3	11.1	10.6
CO_2 concrete and reinforcement [kg/(m year)]	2.2	5.2	2.9	2.4

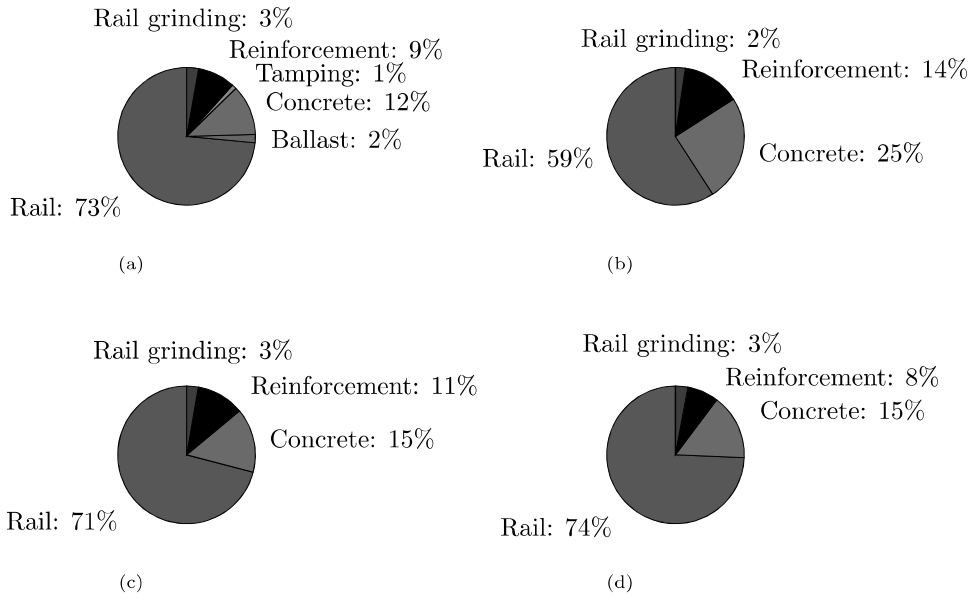

Figure 13. Distribution of CO_2 emission from the production of different materials and maintenance activities considering (a) ballasted track design (b) ST design (c) EN design and (d) 3MB design.

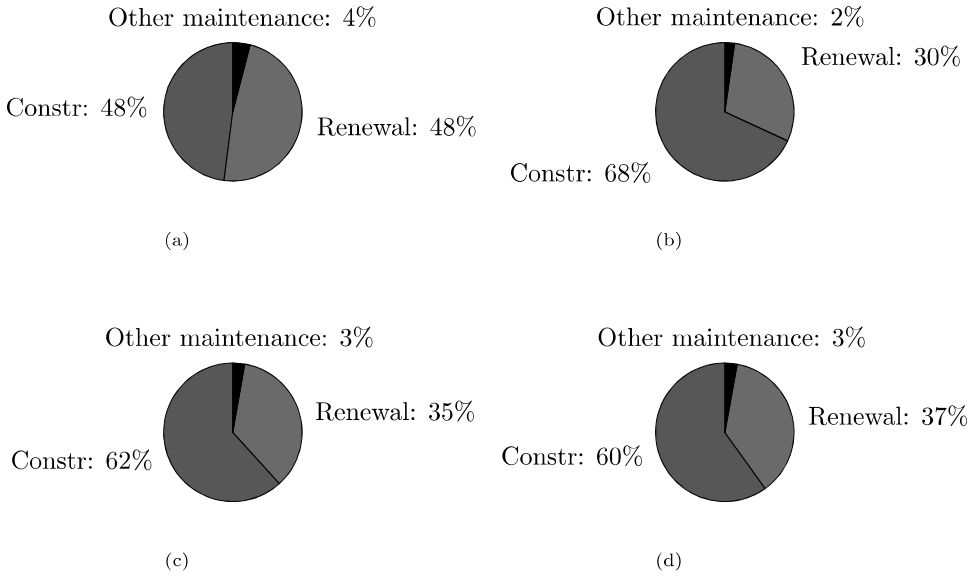

Figure 14. Distribution of CO_2 emission related to the construction (including production), renewal and other maintenance activities for (a) ballasted track design (b) ST design (c) EN design and (d) 3MB design.

5. Conclusions

A ballasted track design has been compared to three different slab track solutions including (i) a slab track design inspired by a system currently available on the market (ii) a slab track design based on the European standard 16432–2 [23] and (iii) the 3MB system developed by ACCIONA, CEMOSA, SYSTRA and INECO [24]. The comparison was performed both in terms of dynamic performance and from an LCA point of view. The simulations of vertical dynamic vehicle–track interaction were performed using 3D models of the vehicle and tracks. The studied excitations included both rail

irregularities (longitudinal level) based on a PSD and wheel flats of varying depth. The LCA was developed to calculate the global warming potential from the different track designs and included all major emission sources.

Below, the main conclusions from the study are given:

1. The 3MB system has a significantly lower static stiffness compared to the other track designs. The main reasons are a lower stiffness between the block and base and a reduced surface area in contact with the foundation compared to the other slab track designs. A similar static stiffness was found for the ballasted track design and the ST and EN slab track designs since a higher rail pad stiffness was used for the ballasted track design. The significantly lower static stiffness of the 3MB design may be problematic in transition zones to other track designs due to the induced track stiffness gradient.
2. For the applied PSD of vertical track irregularity with wavelengths in the interval $1 - 25$ m, the dynamic contribution to the vertical wheel–rail contact force is generally larger for the slab track designs compared to the ballasted track design. The reason for this is that in the frequency range which is excited by the PSD, the ballasted track and the 3MB design (to some extent) have advantageous system receptance characteristics compared to the other designs. Further, similar levels of maximum wheel–rail contact force are obtained for all slab track designs when the track is excited by a high-frequent excitation (in this paper a wheel flat). The corresponding maximum value for the ballasted track design is slightly lower mainly due to a higher rail pad stiffness.
3. A significant difference in the maximum stress of the concrete parts in the different designs was noted. In particular, higher stress levels were observed in the sleepers, in the base slab of the 3MB design and in the panels of the ST and EN designs. For the investigated load cases, when comparing the maximum stress with the maximum flexural tensile strength, it was concluded that stresses in all concrete parts were below the crack initiation level. Regarding the pressure on the foundation, it was concluded that the ballasted track design results in a significantly higher pressure level mostly due to the smaller area in contact with the foundation compared to the slab track designs. Increased pressure levels were also noted for the 3MB design at the locations where two base slabs meet. This effect was not seen for the other slab track designs that use discrete panels but a continuous roadbed. In these designs, low pressure levels with no areas of significantly concentrated pressure levels were noted, which implies that the risk of differential settlement is low.
4. The calculated total level of CO_2 emitted per metre track and year is in the interval $10.5 - 13.3$ kg/(m year) for the studied track designs. The ballasted track emits slightly less CO_2 compared to the other systems while the highest impact is from the ST design in which two layers of reinforced concrete are used. The difference between the designs is, however, not very large since the assumed service life of the concrete parts in the slab track designs is longer than the service life of the sleepers. By comparing different CO_2 emission sources, it was concluded that the production of steel and concrete contributes the most to the total level of CO_2 emission during the service life of the track. In particular, maintenance activities such as rail grinding and tamping is only a small fraction of the total amount of CO_2 emissions.
5. There is a significant difference between the ratio of the environmental cost of construction versus renewal between the designs. For the ballasted track, the environmental cost of renewal is 48% of the overall cost. In contrast, for the ST design that uses reinforced panels and roadbed that are assumed to have a significantly longer life than the concrete sleepers used in a ballasted track design, the corresponding renewal cost is only 30%.

From the abovementioned conclusions, important differences between the studied track designs have been found. As expected, all track designs have advantages and disadvantages. Therefore, it is not possible to conclude that one specific track design is the optimal design in all situations. The most suitable track design depends on how the advantages and disadvantages of the respective track design

are weighted, which may differ between different sites and applications. However, by considering the differences between the track designs highlighted in this paper, the chance of selecting the optimal track design for the specific track location and application is increased.

Acknowledgments

The current study is part of the on-going activities within CHARMEC – Chalmers Railway Mechanics (www.chalmers.se/charmec). Discussions with Prof Jens C. O. Nielsen are gratefully acknowledged. The specifics of the 3MB design were provided by the R&D department at ACCIONA. Parts of the simulations were performed using resources at Chalmers Centre for Computational Science and Engineering (C3SE) provided by the Swedish National Infrastructure for Computing (SNIC).

Disclosure statement

No potential conflict of interest was reported by the author.

Funding

This work was supported by the European Union's Horizon 2020 research and innovation programme in the project In2Track3 under grant agreement no 101012456.

ORCID

Emil Aggestam http://orcid.org/0000-0002-3796-9232

References

[1] Matias SR, Ferreira PA. Railway slab track systems: review and research potentials. Struct Infrastruct Eng. 2020;16(12):1635–1653.
[2] Gautier PE. Slab track: review of existing systems and optimization potentials including very high speed. Constr Build Mater. 2015;92:9–15.
[3] Juanjuan R, Rongshan Y, Ping W, et al. Influence of contact loss underneath concrete underlayer on dynamic performance of prefabricated concrete slab track. Proc Inst Mech Eng F J Rail Rapid Transit. 2017;231(3):345–358.
[4] Zhai W, Wang K, Chen Z, et al. Full-scale multi-functional test platform for investigating mechanical performance of track–subgrade systems of high-speed railways. Railway Eng Sci. 2020;28(3):213–231.
[5] Esveld C. Recent developments in slab track. *European Railway Review*. 2003;9(2):81–85.
[6] Bezin Y, Farrington D, Penny C, et al. The dynamic response of slab track constructions and their benefit with respect to conventional ballasted track. Veh Syst Dyn. 2010;48(S1):175–193.
[7] Steenbergen M, Metrikine A, Esveld C. Assessment of design parameters of a slab track railway system from a dynamic viewpoint. J Sound Vib. 2007;306(1–2):361–371.
[8] Zhai W, Wang K, Cai C. Fundamentals of vehicle–track coupled dynamics. Veh Syst Dyn. 2009;47(11):1349–1376.
[9] Aggestam E *Slab track optimisation considering dynamic train–track interaction*. Ph. D. thesis, Department of Mechanics and Maritime Sciences, Chalmers University of Technology, Gothenburg: Sweden; 2021.
[10] Sadeghi J, Khajehdezfuly A, Esmaeili M, et al. Investigation of rail irregularity effects on wheel/rail dynamic force in slab track: comparison of two and three dimensional models. J Sound Vib. 2016;374:228–244.
[11] Theyssen JS, Aggestam E, Zhu S, et al. Calibration and validation of the dynamic response of two slab track models using data from a full-scale test rig. Eng Struct. 2021;234:111980.
[12] Zhai W, Xia H, Cai C, et al. High-speed train–track–bridge dynamic interactions – part I: theoretical model and numerical simulation. Int J Rail Trans. 2013;1(1–2):3–24.
[13] Zhai W, Wang S, Zhang N, et al. High-speed train–track–bridge dynamic interactions – part II: experimental validation and engineering application. Int J Rail Trans. 2013;1(1–2):25–41.
[14] Luo J, Zhu S, Zhai W. Development of a track dynamics model using Mindlin plate theory and its application to coupled vehicle-floating slab track systems. Mech Syst Signal Process. 2020;140:106641.
[15] Yang J, Zhu S, Zhai W. A novel dynamics model for railway ballastless track with medium-thick slabs. Appl Math Modell. 2020;78:907–931.

[16] Blanco-Lorenzo J, Santamaria J, Vadillo E, et al. Dynamic comparison of different types of slab track and ballasted track using a flexible track model. Proc Inst Mech Eng F J Rail Rapid Transit. 2011;225(6):574–592.
[17] Chen M, Sun Y, Zhu S, et al. Dynamic performance comparison of different types of ballastless tracks using vehicle-track-subgrade coupled dynamics model. Eng Struct. 2021;249:113390.
[18] Ntotsios E, Thompson DJ, Hussein MFM. A comparison of ground vibration due to ballasted and slab tracks. Transp Geotech. 2019;21:100256.
[19] Zhang X, Jeong H, Thompson D, et al. The noise radiated by ballasted and slab tracks. Appl Acoust. 2019;151:193–205.
[20] Milford RL, Allwood JM. Assessing the CO2 impact of current and future rail track in the UK. Transp Res D Transp Environ. 2010;15(2):61–72.
[21] Du G, Karoumi R. Life cycle assessment of a railway bridge: comparison of two superstructure designs. Struct Infrastruct Eng. 2013;9(11):1149–1160.
[22] Pons JJ, Sanchis IV, Franco RI, et al., Life cycle assessment of a railway tracks substructures: comparison of ballast and ballastless rail tracks. *Environmental Impact Assessment Review*. 2020; 85:106444.
[23] EN 16432-2 CEN Standard. Railway applications – ballastless track systems – part 2: system design, subsystems and components. 2017.
[24] In2Track-2. Introductory document to Gransjö demonstrator. 2018.
[25] Nielsen JCO. High-frequency vertical wheel–rail contact forces – validation of a prediction model by field testing. Wear. 2008;265(9–10):1465–1471.
[26] Aggestam E, Nielsen JCO, Lundgren K, et al. Optimisation of slab track design considering dynamic train–track interaction and environmental impact. Eng Struct. 2022;254:113749.
[27] Capacity4Rail. Deliverable D 11.2, design requirements, concepts and prototype test results (intermediate). 2017.
[28] Capacity4Rail. Deliverable D 11.3, design requirements, concepts and prototype test results (final). 2017.
[29] Aggestam E, Nielsen JCO. Simulation of vertical dynamic vehicle–track interaction using a three-dimensional slab track model. Eng Struct. 2020;222:110972.
[30] Aggestam E, Nielsen JCO. Multi-objective optimisation of transition zones between slab track and ballasted track using a genetic algorithm. J Sound Vib. 2019;446:91–112.
[31] Knothe K, Grassie S. Modelling of railway track and vehicle/track interaction at high frequencies. Veh Syst Dyn. 1993;22(3–4):209–262.
[32] Iwnicki S. Manchester benchmarks for rail vehicle simulation. Veh Syst Dyn. 1998;30(3–4):295–313.
[33] Nielsen JCO, Abrahamsson TJS. Coupling of physical and modal components for analysis of moving non-linear dynamic systems on general beam structures. Int J Numer Method Biomed Eng. 1992;33 (9):1843–1859.
[34] Nielsen JCO, Igeland A. Vertical dynamic interaction between train and track – influence of wheel and track imperfections. J Sound Vib. 1995;187(5):825–839.
[35] Aggestam E, Nielsen JCO, Bolmsvik R. Simulation of vertical dynamic vehicle–track interaction using a two-dimensional slab track model. Veh Syst Dyn. 2018;56(11):1633–1657.
[36] Claus H, Schiehlen W. Modeling and simulation of railway bogie structural vibrations. Veh Syst Dyn. 1998;29 (S1):538–552.
[37] EN 13848-6 CEN Standard. Railway applications – track – track geometry quality – part 6: characterisation of track geometry quality. 2014.
[38] Wu TX, Thompson DJ. A hybrid model for the noise generation due to railway wheel flats. J Sound Vib. 2002;251(1):115–139.
[39] voestalpine Schienen GmbH. Environmental Product declaration – rails for high-speed railways, mixed traffic, heavy loads, urban public transportation, crane and construction rails. 2019.
[40] Hjulsbro Steel AB. Environmental product declaration (EPD) – PC-strand – prestressed steel for reinforcement of concrete (single supplier). 2020.
[41] Cementa AB, HeidelbergCement Group. Environmental Product Declaration (EPD) Portland Fly Ash Cement CEM II/A-V 42.5 N. 2016.
[42] Grassie S, Gregory R, Harrison D, et al. The dynamic response of railway track to high frequency vertical excitation. J Mech Eng Sci. 1982;24(2):77–90.
[43] Thompson D. Railway noise and vibration: mechanisms, modelling and means of control. Oxford: Elsevier; 2008.
[44] Bolmsvik R, Nielsen JCO, and Singhal AK. Guideline for design optimization and production of pre-stressed concrete railway sleepers. In: Technical report. Gothenburg: Sweden: Department of Applied Mechanics, Chalmers University of Technology; 2011 1–82.
[45] EN 1992-1-1 CEN Standard. Eurocode 2: design of concrete structures – part 1-1: general rules and rules for building. 2004.
[46] Pieringer A, Kropp W, Nielsen JC. The influence of contact modelling on simulated wheel/rail interaction due to wheel flats. Wear. 2014;314(1–2):273–281.